Welding in the World (2019) 63:161–166
https://doi.org/10.1007/s40194-018-0646-y

RESEARCH PAPER

Uniaxial compression properties of fusion zone martensite in resistance spot-weld for QP980 steel

Chunlei Fan[1,2] · Bohan Ma[2] · Danian Chen[2] · Gaotao Deng[2] · Huanran Wang[2] · Dongfang Ma[2]

Received: 10 December 2017 / Accepted: 22 August 2018 / Published online: 5 September 2018

Abstract

The cross-sectional micrograph, microhardness profile, and microstructures of the resistance spot-weld (RSW) for QP980 steel are shown to reveal the effects of the content and tempering of the martensite in the fusion zone (FZ) and the heat-affected zone (HAZ) on the microhardness profile of the RSW. It is indicated that the transient peak temperature above the critical temperature during the welding thermal cycle induces the significant variations of material and mechanical properties in the FZ and HAZ. The quasi-static uniaxial compression stress-strain curve of the FZ martensite in the RSW for QP980 steel is obtained with digital image correlation (DIC) and compared with that of two micropillars of martensite phase in the base material (BM) of the RSW for QP980 steel which was given by Srivastava et al. It is attributed to the welding thermal cycle different from QP980 steel heat treatment that the flow stress of the FZ martensite in the RSW is higher than that of the martensite phase in the BM. The dynamic uniaxial compression experiments for the FZ martensite in the RSW for QP980 steel are performed on a modified split Hopkinson pressure bar (SHPB), in which the reflected and transmitted waves are improved. A dynamic compression constitutive equation is presented by analyzing the results of the quasi-static and dynamic uniaxial compression experiments. A Swift law for martensite phase is extended to high strain rates to describe the weak strain-rate dependence of the dynamic compression behaviors of the FZ martensite in the RSW for QP980 steel.

Keywords Resistance spot-weld · Fusion zone · Uniaxial compression · Quasi-static and dynamic · Constitutive equation

1 Introduction

In 2012, quenching and partitioning (QP) steel with a tensile strength of 980 MPa was successfully commercialized by Baosteel [15]. Wang and Speer [16] overviewed the excellent balance between ultrahigh strength and high ductility of QP steel. Srivastava et al. [12] developed a microstructure-based model to study the mechanisms of deformation in QP980 steel. Yang et al. [19] investigated the histories of strain and strain rate for QP980 steel by using an interruption mechanism for tensile split Hopkinson bar experiments. Transmission electron microscopy and synchrotron X-ray diffraction were conducted [19] to analyze the effects of strain and strain rate on the martensitic transformation of retained austenite. The QP980 steel can be successfully welded with resistance spot welding (RSW). Wang et al. [17] performed the microstructural characterization, microhardness tests, and tensile and fatigue tests of spot welded QP980 steel using tensile-shear and cross-tension specimens. Ma et al. [7] investigated the ultrahigh-speed tests for purely opening RSW of QP980 steel by using plane tensile pulses. Fan et al. [4] reported the spall strength of the RSW for QP980 steel.

In this paper, the uniaxial compression properties of the fusion zone martensite in the RSW for QP980 steel at various strain rates are investigated. The quasi-static uniaxial compression stress-strain curve of the fusion zone martensite in the RSW is obtained with digital image correlation (DIC) technique and compared with the curves of two micropillars of martensite phase for QP980 steel given by Srivastava et al. [12]. It is indicated that due to the welding thermal cycle different from QP steel heat treatment, the flow stress of the

Recommended for publication by Commission III - Resistance Welding, Solid State Welding, and Allied Joining Process

✉ Danian Chen
chdnch@nbu.edu.cn

[1] Zhejiang Industry Polytechnic College, Shaoxing 312006, Zhejiang, China

[2] Mechanics and Material Science Research Center, Ningbo University, Ningbo 315211, Zhejiang, China

Table 1 Resistance spot welding parameters for QP980 steel

Welder	Weld electrode	Thickness of base metal (mm)	Electrode force (kN)	Welding current (A)	Weld time (ms)
Medium-frequency direct current	Copper	1.2	3.6	6000	170

fusion zone martensite in the RSW is higher than that of the martensite phase in the base metal of the RSW for QP980 steel. The dynamic uniaxial compression experiments for the fusion zone martensite in the RSW are performed on a modified split Hopkinson pressure bar (SHPB) in which the reflected and transmitted waves are improved. A Swift law for martensite phases is extended to high strain rates to describe the weak strain-rate dependence of the dynamic compression behaviors of the fusion zone martensite in the RSW for QP980 steel.

1.1 Experiments

The resistance spot welding for 1.2-mm QP980 steel is accomplished using a medium frequency direct current welding machine with the welding parameters listed in Table 1. In order to investigate the yield strength of the materials in the RSW for QP980 steel, the cross-sectional micrograph, microhardness profile, and microstructures of the RSW for QP980 steel are shown in Fig. 1a–c, respectively. Figure 1c shows that the microstructures in fusion zone (FZ) and heat-affected zone (HAZ) are different from pre-existing microstructures in base metal (BM) due to the rapid heating and subsequent cooling during welding. In fact, the materials in the FZ and HAZ of the RSW are martensite phases as shown in Fig. 1c. The tempering of martensite has been documented as the main cause of softening in martensitic steels. Hernandez et al. [5] found that the decomposed martensite was the major contributor to measured softening at microscale. Figure 1b shows a microhardness profile obtained across the welded region from

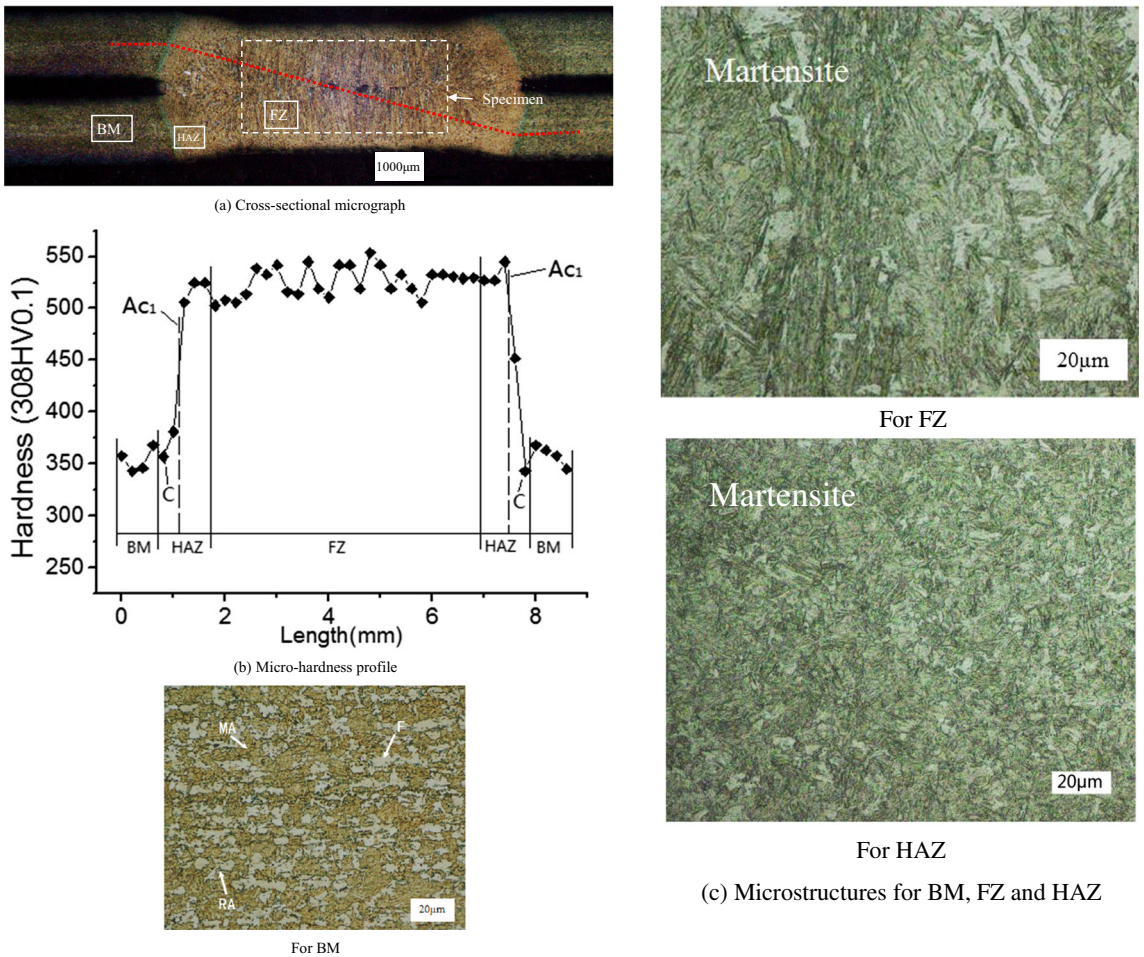

Fig. 1 The spot-weld cross-sectional micrograph, microhardness profile, and microstructures for 1.2-mm QP980 steel. MA (martensite-austenite), RA (retained austenite), and F (ferrite)

the BM through the HAZ and FZ. In the literature [5, 8, 9, 18], the reduction in Vicker's microhardness has been studied in dual phase (DP) steel when subjected to rapid thermal cycles during resistance spot welding. During the welding thermal cycle, the martensite and part of the ferrite are briefly transformed to austenite at a critical temperature T_c and then retransformed to new martensite during cooling. The local post-weld martensite content in the critical HAZ could be above the level in the BM, leading to higher local hardness. A reduction in hardness with respect to BM could be observed in the sub-critical HAZ. Maximum softening at c in Fig. 1b is located just below the line of the critical temperature T_c.

The significant variations of material and mechanical properties in the FZ and HAZ render extremely challenging to the development of material models capable of capturing the behavior of the FZ and HAZ. Some test results [13] of the FZ and HAZ of the RSW for DP steel have been obtained with a novel strain-mapping technique based on DIC. The newly developed DIC technique is used to measure the strains of the FZ martensite specimen in the RSW for QP980 steel as shown in Fig. 1a during quasi-static uniaxial compression testing as shown in Fig. 2a. The shape of specimens is cylinder. The specimen height is 2.10 mm and has a bore diameter of 3.0 mm. The material of special blocks is tungsten carbide with a thickness of 7.85 mm and a diameter of 19.5 mm. The quasi-static uniaxial compression stress-strain curve of the FZ martensite in the RSW for QP980 steel is presented in Fig. 3. The dynamic uniaxial compression experiments for these specimens are performed on a modified SHPB. These specimens with smaller diameter than the bars and higher hardness than the bars are to indent the bars in the SHPB tests producing a type of bar misalignment. Kariem et al. [6] studied the distorted signal generated by different misalignments in SHPB experiments. We design proper sandwich (as shown in Fig. 2b) between the specimen and the bars to improve the reflected and transmitted waves as shown in Fig. 4, in which the yellow signal is the incident and reflected wave, the blue signal indicates the transmitted wave, X-axis indicates time, and Y-axis is electric voltage. The dynamic uniaxial compression stress-strain curves of the FZ martensite specimen in the RSW for QP980 steel at various strain rates are shown in Fig. 5. It is revealed that the strain-rate dependence of the dynamic uniaxial compression behavior of the FZ martensite in the RSW for QP980 steel is rather weak according to Fig. 5.

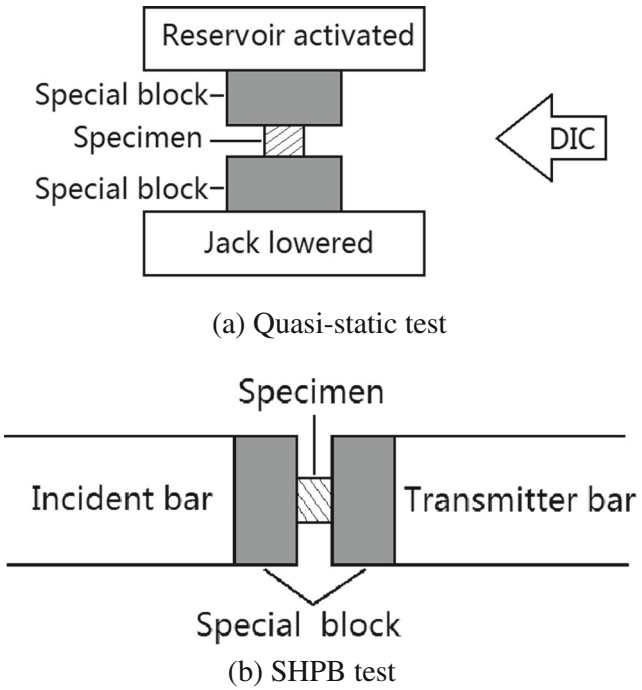

Fig. 2 The designed proper sandwich of the quasi-static and SHPB tests for the FZ martensite specimen in the RSW of QP980 steel

2 Analyses

We [4] have revealed the martensite phases in the FZ and HAZ of the as-received RSW for QP980 steel in all details with a number of micrographs. Srivastava et al. [12] have given the experimental and calculated uniaxial compression stress-strain curves of two micropillars of martensite phase in QP980 steel, which are also shown in Fig. 3. The experimental compression stress-strain curves of micropillar extracted from the individual martensite particles were obtained [12] using a flat-punch nanoindenter while calculated using five material parameters including the initial dislocation density. It is obvious from Fig. 3 that the quasi-static uniaxial compression stress-strain curve of the FZ martensite in RSW for QP980 steel is different from that of the micropillars of martensite phase in QP980 steel. Obviously, it is due to the welding thermal cycle different from the QP980 steel heat treatment that the flow stress of the FZ martensite in the RSW is higher than that of the martensite phase in the BM. The behavior of martensite phase can be determined by tests on steels

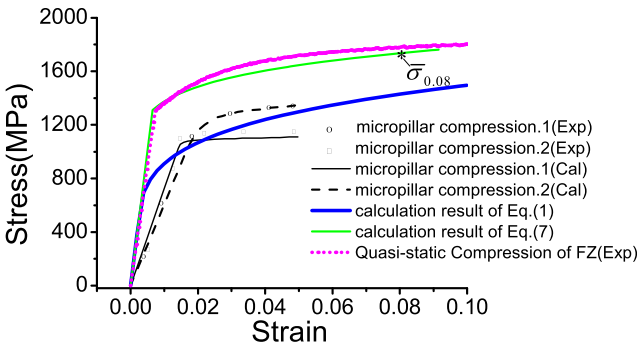

Fig. 3 The quasi-static uniaxial compression stress-strain curve of the FZ martensite in the RSW for QP980 steel and the experimental and calculated compression stress-strain curves[3] of two micropillars of martensite phase in QP980 steel

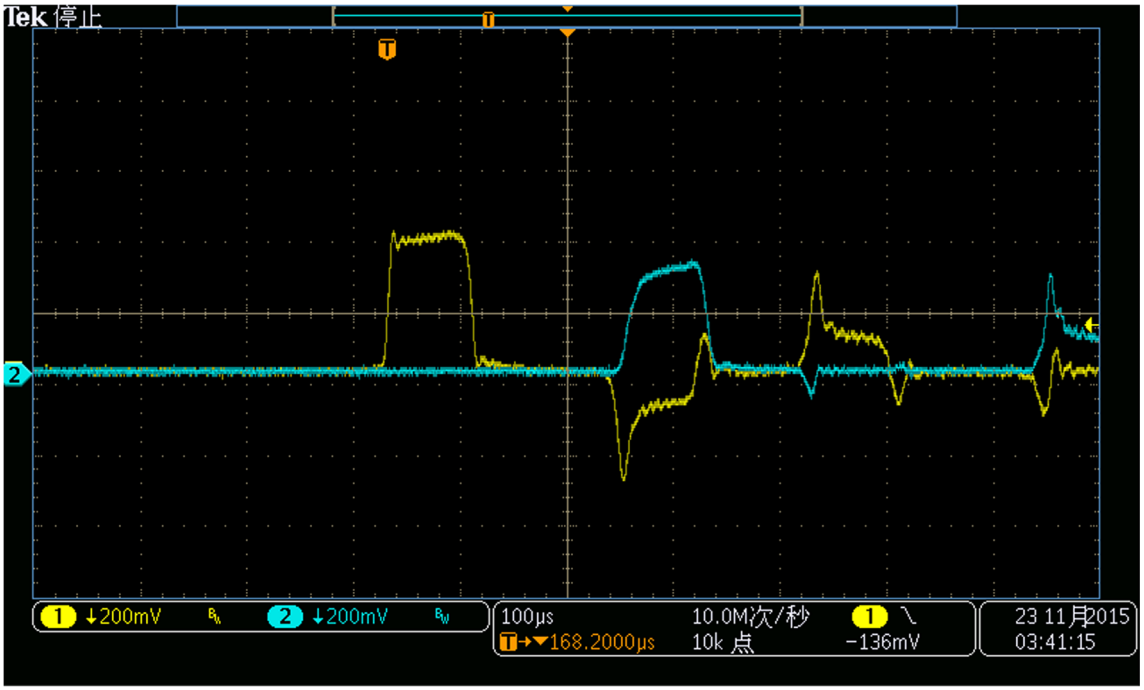

Fig. 4 Typical oscilloscope record of the modified SHPB test for the FZ martensite specimen in the RSW for QP980 steel

consisting of martensite phase. This is achievable by heating the steel to the required temperature and then cooling at controlled rates using the time-temperature transformation diagram to get the martensite phase. The martensite-phase steel can be tested in compression or tension to obtain the characteristic behavior of the martensite phase. However, the reported martensite phase properties vary significantly in the open literature [2, 3]. Tomata et al. [14] represented a Swift law for martensite phase:

$$\sigma_e = a\left(b + \varepsilon_p\right)^N \tag{1}$$

where σ_e is the plastic flow stress, ε_p is the accumulated plastic strain. The parameters a, b, and N are derived systematically from the stress-strain curve of martensite phase [10, 11]. $a = 8590c + 1830\text{MPa}$, $b = 0.0001$, $N = 0.763c + 0.153$, and c is carbon composition (mass %). For martensite in QP980 steel, $c = 0.06\%$, $a = 2380\text{MPa}$, $b = 0.0001$, and $N = 0.2$, the stress-strain curve calculated from Eq. (1) is also shown in Fig. 3.

The relation of Vicker's hardness to the $\sigma_{0.08}$ is given [1] by

$$HV = 3\sigma_{0.08} \tag{2}$$

We can calculate uniaxial $\overline{\sigma}_{0.08}$ for the FZ martensite in the RSW for QP980 steel as follows:

$$\overline{\sigma}_{0.08} = \frac{1}{n}\sum_{i=1}^{n}\left(\sigma_{0.08}\right)_i = 1750\text{MPa} \tag{3}$$

where $(\sigma_{0.08})_i$ is $\sigma_{0.08}$ at the indentation points, n=1, 2…25, 26, and$(\sigma_{0.08})_i = 1667\sim1840\text{MPa}$ in the FZ. The calculated $\overline{\sigma}_{0.08}$ is also shown in Fig. 3.

Most metallic material's plastic behaviors can be expressed by a power law. Material's elasto-plastic behavior can be described as:

$$\sigma = \begin{cases} E\varepsilon & for\ \sigma \le \sigma_{y0} \\ \sigma_{y0}\left(1+\frac{E}{\sigma_{y0}}\varepsilon_p\right)^m & for\ \sigma \ge \sigma_{y0} \end{cases} \tag{4}$$

where E is the elastic modulus, σ_{y0} is the initial yield strength, and m is the hardening exponent. We assume the elasto-plastic behavior $\overline{\sigma}$ of the FZ martensite in the RSW for QP980 steel to satisfy Eq. (4), then m can be determined from $\overline{\sigma}_{0.08}$, E, and σ_{y0}. According to Fig. 3, E=200 GPa, and σ_{y0}=1310 MPa for the FZ martensite in the RSW for QP980 steel. Therefore, m=0.112 and $\overline{\sigma}$ can be described as:

$$\overline{\sigma}(\text{MPa}) = \begin{cases} 200000\varepsilon & for\ \sigma \le 1310\text{MPa} \\ 1310\left(1 + 153\varepsilon_p\right)^{0.112} & for\ \sigma \ge 1310\text{MPa} \end{cases} \tag{5}$$

which is shown in Fig. 3.

In fact, Eq. (5) is a Swift law, and we extend the Swift law to high strain rates. Taking strain rate effect into consideration, a strain rate effect term is added to Eq. (5), and the dynamic compression constitutive equation of the FZ martensite in the RSW for QP980 steel is obtained, that is Eq. (6), which is presented by analyzing the quasi-static and dynamic uniaxial compression experimental results:

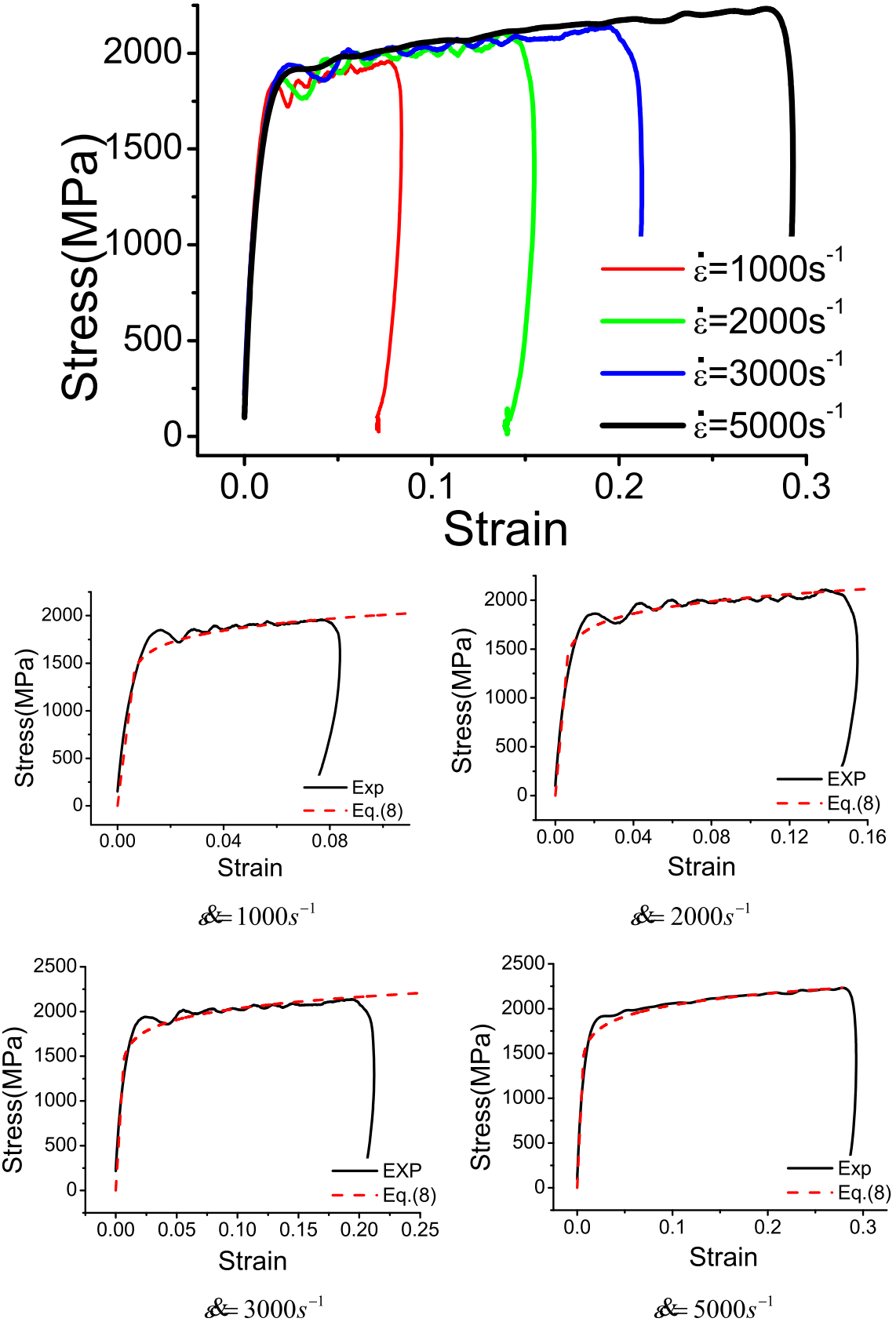

Fig. 5 The dynamic uniaxial compression stress-strain curves of the FZ martensite in the RSW for QP980 steel at various strain rates

$$\sigma_e = A\left(1 + B\varepsilon_p\right)^{n'}\left(1 + C\ln\frac{\dot{\varepsilon}_p}{\dot{\varepsilon}_0}\right) \quad (6)$$

where A=1310 MPa, B=153, n'=0.112, and $\dot{\varepsilon}_p$ is the strain rate, $\dot{\varepsilon}_0 = 1.0\ s^{-1}$, C=0.015. The stress-strain curves at high strain rates described with Eq. (6) are compared with the experimental results in Fig. 5.

3 Conclusions

1) The cross-sectional micrograph, microhardness profile, and microstructures of the RSW for QP980 steel are shown to reveal the effects of the content and tempering of the martensite in the FZ and HAZ on the microhardness profile of the RSW. It is indicated that during the welding thermal cycle, the transient peak temperature above the critical temperature induces the significant variations of material and mechanical properties in the FZ and HAZ.
2) The quasi-static uniaxial compression stress-strain curve of the FZ martensite in the RSW for QP980 steel is obtained with DIC technique and compared with the experimental and calculated uniaxial compression stress-strain curves of two micropillars of martensite phase in the BM of the RSW for QP980 steel, which was given by Srivastava et al. [12]. It is attributed to the welding thermal cycle different from the QP980 steel heat treatment that the flow stress of the FZ martensite in the RSW is higher than that of the martensite phase in the BM.
3) The dynamic uniaxial compression experiments for the FZ martensite in the RSW for QP980 steel are performed on a modified SHPB in which the reflected and transmitted waves are improved. A dynamic compression constitutive equation for the FZ martensite in the RSW for QP980 steel is presented analyzing the results of the quasi-static and dynamic uniaxial compression experiments. A Swift law for martensite phase is extended to high strain rates to describe the weak strain-rate dependence of the dynamic compression behaviors of the FZ martensite in the RSW for QP980 steel.

Funding information This study was financially supported by the National Nature Science Foundation of China under Grant No. 11372149.

References

1. Cahoon JR, Broughton WH, Kutzak AR (1971) The determination of yield strength from hardness measurements. Metall Trans 2(7): 1979–1983
2. Choi KS, Liu WN, Sun X, Khaleel MA (2009) Microstructure-based constitutive modeling of TRIP steel: prediction of ductility and failure modes under different loading conditions. Acta Mater 57:2592–2604
3. Delannay L, Jacques P, Pardoen T (2008) Modelling of the plastic flow of trip-aided multiphase steel based on an incremental mean-field approach. Int J Solids Struct 45:1825–1843
4. Fan CL, Ma BH, Chen DN, Wang HR, Ma DF (2016) Spall strength of resistance spot weld for QP steel. Chin Phys Lett 33: 036201-036201-5
5. Hernandez VHB, Panda SK, Kuntz ML, Zhou Y (2010) Nanoindentation and microstructure analysis of resistance spot welded dual phase steel. Materials Let 64:207–210
6. Kariem MA, Beynon JH, Ruan D (2012) Misalignment effect in the split Hopkinson pressure bar technique. Int J Impact Eng 47:60–70
7. Ma BH, Fan CL, Chen DN, Wang HR, Zhou FH (2014) An investigation of the dynamic separation of spot welds under plane tensile pulses. J Appl Phys 116:053503-053503-9
8. Marya M, Wang K, Hector LG, Gayden X (2006) Tensile-shear forces and fracture modes in single and multiple weld specimens in dual-phase steels. J Manuf Sci Technol 128:287–298
9. Panda SK, Sreenivassan N, Kuntz ML, Zhou Y (2008) Numerical simulations and experimental results of tensile test behavior of laser butt welded DP980 steels. J Eng Mater Tech 130:531–534
10. Pickering FB (1981) Physical metallurgy and design of steels
11. Rauch GC, Leslie WC (1972) The extent and nature of the strength-differential effect in steels. Metall Trans 3:377–389
12. Srivastava A, Ghassemi-Armaki H, Sung H, Chen P, Kumar S, Bower AF (2015) Micromechanics of plastic deformation and phase transformation in a three-phase TRIP-assisted advanced high strength steel: experiments and modeling. J Mech Phys Solids 78: 46–69
13. Tong W, Tao H, Jiang X, Zhang N, Marya MP (2005) Deformation and fracture of miniature tensile bars with resistance-spot-weld microstructures. Metall Mater Trans A 36:2651–2669
14. Tomata Y, Umemoto M, Komatsubara N, Hiramatsu A, Nakajima N, Moriya A, Watanabe T, Nanba S, Anan G, Kunishige K, Higo Y, Miyahara M (1992) Prediction of mechanical properties of multi-phase steels based on stress-strain curves. ISIJ Int 32:343–349
15. Wang L, Jin X, Qian H (2011) Recent development of galvanizing sheet steels in Baosteel. In proceedings of Galvatech 2011, Eight International Conference on zinc and Zinc Alloy Coated sheet steel, Genova
16. Wang L, Speer JG (2013) Quenching and partitioning steel heat treatment. Metallogr Microstruct Anal 2:268–281
17. Wang B, Duan QQ, Yao G, Pang JC, Li XW, Wang L, Zhang ZF (2014) Investigation on fatigue fracture behaviors of spot welded Q&P980 steel. Int J Fatigue 66:20–28
18. Xia M, Biro E, Tian Z, Zhou Y (2008) Effects of heat input and martensite on HAZ softening in laser welding of dual phase steels. ISIJ Int 48:809–814
19. Yang X, LGJr H, Wang J (2014) A combined theoretical/experimental approach for reducing ringing artifacts in low dynamic testing with servo-hydraulic load frames. Exp Mech 54:775–789